Chemical Science

EDGE ARTICLE

View Article Online
View Journal | View Issue

Cite this: *Chem. Sci.*, 2015, **6**, 4723

Experimental observation of TiN_{12}^+ cluster and theoretical investigation of its stable and metastable isomers†

Ke-Wei Ding,‡[a] Xiao-Wei Li,‡[bc] Hong-Guang Xu,[d] Tao-Qi Li,*[a] Zhong-Xue Ge,*[a] Qian Wang*[c] and Wei-Jun Zheng*[d]

Received 27th March 2015
Accepted 9th May 2015

DOI: 10.1039/c5sc01103e

www.rsc.org/chemicalscience

TiN_n^+ clusters were generated by laser ablation and analyzed experimentally by mass spectrometry. The results showed that the mass peak of the TiN_{12}^+ cluster is dominant in the spectrum. The TiN_{12}^+ cluster was further investigated by photodissociation experiments with 266, 532 and 1064 nm photons. Density functional calculations were conducted to investigate stable structures of TiN_{12}^+ and the corresponding neutral cluster, TiN_{12}. The theoretical calculations found that the most stable structure of TiN_{12}^+ is $Ti(N_2)_6^+$ with O_h symmetry. The calculated binding energy is in good agreement with that obtained from the photodissociation experiments. The most stable structure of neutral TiN_{12} is $Ti(N_2)_6$ with D_{3d} symmetry. The Ti–N bond strengths are greater than 0.94 eV in both $Ti(N_2)_6^+$ and its neutral counterpart. The interaction between Ti and N_2 weakens the N–N bond significantly. For neutral TiN_{12}, the $Ti(N_3)_4$ azide, the N_5TiN_7 sandwich structure and the N_6TiN_6 structure are much higher in energy than the $Ti(N_2)_6$ complex. The DFT calculations predicted that the decomposition of $Ti(N_3)_4$, N_5TiN_7, and N_6TiN_6 into a Ti atom and six N_2 molecules can release energies of about 139, 857, and 978 kJ mol^{-1} respectively.

1 Introduction

Nitrogen-rich and all-nitrogen compounds are potential candidates for high energy density materials (HEDMs).[1–6] Despite numerous theoretical and experimental efforts aimed at all-nitrogen compounds, only a few attempts, for example the synthesis of N_5^+ salts[7] and the detection of N_4 with a lifetime of only about 1 microsecond,[8] have been successful. A less challenging goal might be to produce nitrogen-rich species containing one or more other atoms. Thus, metal-doped nitrogen clusters have drawn increasing attention in recent years because of their diversiform structures and predicted relatively high stabilities.[9–11] These clusters can also be considered as good models for understanding the formation and properties of nitrogen-rich compounds at the molecular level.

Due to their importance in understanding metal–nitrogen interactions, metal–nitrogen complexes have been extensively investigated by a variety of experimental techniques in recent decades. Andrews and co-workers investigated Fe–N_2, Sc–N_2, Os–N_2, and Ru–N_2 complexes with matrix-isolated infrared spectroscopy[12–15] and found that an Os atom can insert directly into the dinitrogen bond to form bent NOsN. Duncan and co-workers investigated In–N_2 and Al–N_2 complexes by photoionization spectroscopy,[16,17] and studied Mg^+–N_2, Ca^+–N_2, $Nb^+(N_2)_n$, and $V^+(N_2)_n$ complexes using photodissociation spectroscopy.[18–21] Dagdigian and co-workers studied the electronic states of an Al–N_2 complex with laser-induced fluorescence spectroscopy.[22]

Many kinds of binary azides have been prepared and characterized experimentally, and have also been investigated by theoretical calculations. $B(N_3)_3$ was isolated in a low-temperature argon matrix and characterized by FTIR spectroscopy;[23] recently, it was also identified by a combination of VUV photoelectron spectroscopy and outer valence Green's functional calculations.[24] Binary azides of Group 4 elements (such as Ti),[25] Group 5 elements (V, Nb, and Ta),[26–28] Group 6 elements (Mo and W),[29] Group 14 elements (Si and Ge),[30–32] Group 15 and 16 elements (P, Bi, Se, and Te)[33–36] were synthesized and isolated experimentally, and were characterized by NMR spectroscopy. Some of them were also examined by infrared and/or Raman spectroscopy, and verified by theoretical calculations. Gagliardi and Pyykkö studied the Group 4 tetra-azides $M(N_3)_4$ (M = Ti–Hf, Th) by theoretical calculations.[37] Li and Duan investigated the

[a]*Xi'an Modern Chemistry Research Institute, Xi'an 710065, China. E-mail: thankli64@163.com; gzx204@sina.com*

[b]*National Laboratory of Mineral Materials, School of Materials Science and Technology, China University of Geosciences, Beijing 100083, China*

[c]*Center for Applied Physics and Technology, College of Engineering, Peking University, and IFSA Collaborative Innovation Center, Ministry of Education, Beijing 100871, China. E-mail: qianwang2@pku.edu.cn*

[d]*State Key Laboratory of Molecular Reaction Dynamics, Institute of Chemistry, Chinese Academy of Sciences, Beijing 100190, China. E-mail: zhengwj@iccas.ac.cn*

† Electronic supplementary information (ESI) available: NBO data for TiN_2, TiN_2^+, TiN_{12} and TiN_{12}^+. See DOI: 10.1039/c5sc01103e

‡ K.-W. Ding and X.-W. Li contributed equally to this work.

structures and stabilities of a series of tri-azides $M(N_3)_3$ (M = Sc, Y, La, B, Al, Ga, In, Tl) and tetra-azides $M(N_3)_4$ (M = Ti, Zr, Hf, C, Si, Ge, Sn, Pb) using density functional theory calculations.[38]

Many researchers have used theoretical chemistry to investigate species containing polynitrogen rings. The theoretical calculations of Gagliardi and Pyykkö found that ScN_7 has a local minimum with C_{7v} symmetry,[9] and that the sandwich structures of N_5MN_7 (M = Ti, Zr, Hf, Th) are locally stable.[10] Other species with polynitrogen rings, such as CsN_7Ba[39] and MN_6 (M = Ti, Zr, Hf, Th),[40] were also investigated theoretically. Theoretical calculations also predicted the possible existence of high-energy nitrogen-rich pentazolides with a very large nitrogen-to-element ratio, such as $[M(N_5)_8]^{2-}$ (M = Cr, Mo, W).[11] After that, Duan and Li investigated a series of polynitrogen ring species (ScN_6^-, TiN_6, VN_6^+, Ca_2N_6, and ScN_6Cu) using density functional theory calculations.[41] Jin and Ding calculated the sandwich structures of $[N_3NiN_3]^{2-}$ and $[N_3MN_5]^q$ [(M, q) = (Ni, 0), (Co, −1), (Fe, −2)] using density functional theory.[42,43] Very recently, an investigation of stable high pressure phases of potassium azide using the first-principles method and the evolutionary algorithm suggested that planar N_6 rings may be formed in potassium azide at a pressure of 100 GPa.[44]

Overall, the previous experimental and theoretical studies have shown that metal–nitrogen clusters may exist in the forms of M–$(N_2)_n$ complexes, binary azides, or polynitrogen ring structures. Whether they are energy-rich or not, they are of great general interest. In this work, we investigated the TiN_{12}^+ cluster by laser ablation and photodissociation experiments coupled with density functional calculations, in order to gain an insight into the geometric and electronic properties of the most stable TiN_{12}^+ cluster, as well as its neutral counterpart. The relative stabilities of the polyazide and polynitrogen ring isomers were also investigated by density functional calculations.

2 Experimental and theoretical methods

2.1 Experimental method

The experiments were conducted on a home-built apparatus equipped with a laser vaporization cluster source and a reflectron time-of-flight mass spectrometer (RTOF-MS), which has been described elsewhere.[45] Briefly, the TiN_{12}^+ cluster ions were generated in the laser vaporization source by laser ablation of a rotating and translating disk target of a mixture of Ti and BN (13 mm diameter, Ti : BN mole ratio = 2 : 1) with the second harmonic of a nanosecond Nd:YAG laser (Continuum Surelite II-10). A typical laser power used in this work is about 10 mJ per pulse. Nitrogen gas with ~4 atm back pressure was allowed to expand into the source through a pulsed valve (General Valve Series 9) to provide nitrogen for cluster formation and to cool the formed clusters. The masses of the generated cluster ions were analyzed with the RTOF-MS. The TiN_{12}^+ cluster ions were further investigated *via* photodissociation experiments. During the photodissociation experiments, the TiN_{12}^+ ions were selected with a pulsed mass-gate at the first space focus point of the RTOF-MS, decelerated with a DC electric field, and then dissociated with 266, 532, and 1064 nm photons from another nanosecond Nd:YAG laser (Continuum Surelite II-10). The fragment ions and parent ions were then re-accelerated toward the reflectron zone and reflected to the microchannel plate (MCP) detector. The output from the MCP detector was amplified with a broadband amplifier and recorded with a 200 MHz digital card. The digitalized data were collected on a laboratory computer with home-made software.

2.2 Computational methods

The theoretical calculations were carried out using GAUSSIAN 09 code.[46] Geometry optimization and frequency analysis were performed at the B3LYP/6-31G* level.[47,48] The ionization energy of Ti and the bond length of the N_2 molecule were calculated to verify the accuracy of our method. The calculated ionization energy of Ti is about 656 kJ mol^{-1} and the N–N bond length is about 1.10 Å, which are consistent with the experimental values of 658.8 kJ mol^{-1} and 1.0977 Å.[49] The binding energy is defined as (n is the number of N_2 molecules):

$$E_{b1} = -[E(TiN_{2n}) - E(Ti) - n \times E(N_2)]/n \text{ (for neutral clusters)}$$

$$E_{b2} = -[E(TiN_{2n}^+) - E(Ti^+) - n \times E(N_2)]/n \text{ (for ionic clusters)}$$

To gain further insight into the interactions between the N_2 molecules and Ti or Ti^+, we performed natural bond orbital (NBO) analysis,[50] in which the electronic wave function is interpreted in terms of a set of occupied Lewis orbitals and a set of unoccupied non-Lewis delocalized orbitals. For each donor NBO (i) and acceptor NBO (j), the stabilization energy E_2 associated with charge transfer $i \rightarrow j$ is given by

$$E_2 = \Delta E_{ij} = q_i \left[\frac{F(i,j)^2}{\varepsilon_j - \varepsilon_i}\right]$$

where q_i is the donor orbital occupancy, ε_i and ε_j are diagonal elements (orbital energies), and $F(i, j)$ is the off-diagonal NBO Fock matrix element.

3 Experimental results

Fig. 1 shows a typical mass spectrum of the clusters generated in our experiments. It can be seen that the predominant mass peaks correspond to Ti^+ and TiN_{12}^+. It is very interesting that there are no mass peaks due to other TiN_n^+ clusters. This indicates that TiN_{12}^+ may have the most stable or symmetric structure in comparison with other clusters. In addition to the mass peak of TiN_{12}^+, we also observed weak mass peaks corresponding to $TiON_8^+$, $TiON_{10}^+$, and $TiO_2N_9^+$ in the mass spectrum. The detection of $TiON_{10}^+$ is similar to the formation of $TiO^+(N_2)_5$ by gas phase clustering of N_2 molecules on TiO^+ reported by Daly and El-Shall.[51]

The photodissociation of TiN_{12}^+ was conducted using 266, 532 and 1064 nm photons. No fragment ions were observed when TiN_{12}^+ was photodissociated by 1064 nm photons. The photodissociation mass spectra of TiN_{12}^+ at 532 and 266 nm

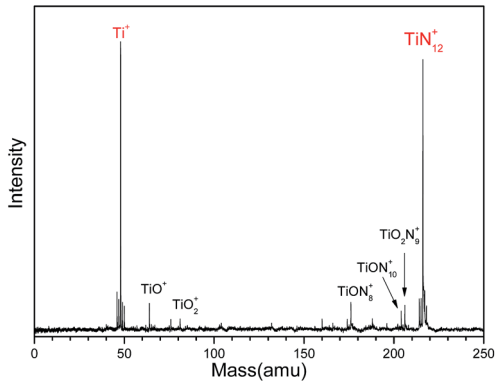

Fig. 1 Typical mass spectrum of Ti–N clusters generated by laser ablation of a Ti : BN mixture target.

are shown in Fig. 2. TiN_8^+, TiN_6^+, TiN_4^+, TiN_2^+ and Ti^+ fragment ions were produced when TiN_{12}^+ was photodissociated by 532 nm photons, and the TiN_6^+ fragment had the highest abundance. This indicates that TiN_{12}^+ can lose at least 4 nitrogen atoms, and that the main dissociation channel when TiN_{12}^+ was photodissociated by 532 nm photons was the loss of 6 nitrogen atoms. The fragment ions observed when TiN_{12}^+ was photodissociated by 266 nm photons were TiN_4^+, TiN_2^+, and Ti^+, which shows that TiN_{12}^+ can lose at least 8 nitrogen atoms.

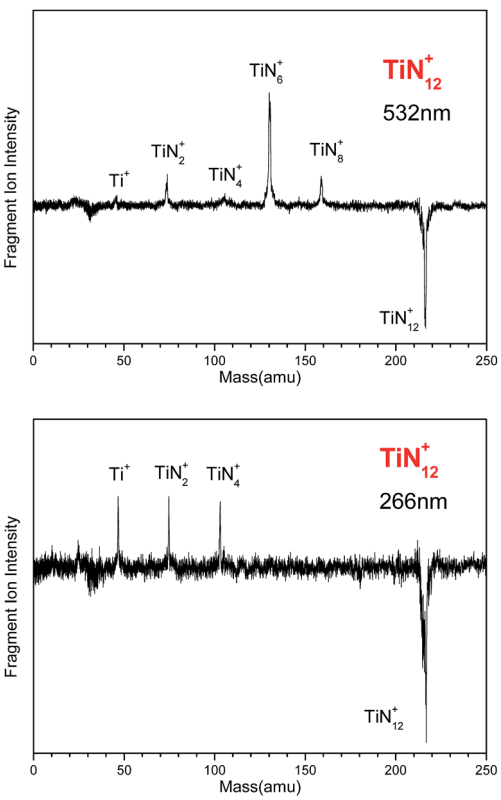

Fig. 2 Photodissociation mass spectra of the TiN_{12}^+ cluster at 532 and 266 nm.

4 Theoretical results

We started with one N_2 molecule bonded to Ti and Ti^+. We calculated both the end-on linear structure and the side-on triangular structure, and found that for TiN_2 the end-on linear geometry is 0.34 eV lower in energy than the side-on geometry, while for TiN_2^+ the two configurations are almost degenerate. The binding energies of the end-on linear configurations were calculated to be 0.25 and 0.93 eV for TiN_2 and TiN_2^+, respectively. TiN_2 was found to have a magnetic moment of 4.0 μ_B, a Ti–N bond length of 1.94 Å, and a N–N bond length of 1.15 Å. While for TiN_2^+, the magnetic moment is 3.0 μ_B, the Ti–N bond length is 2.18 Å, and the N–N bond length is 1.11 Å.

To investigate the stable states of TiN_{12} and TiN_{12}^+, we selected six initial geometrical configurations consisting of one Ti and six N_2 molecules (Fig. 3, I_1–I_6), and two structures consisting of one Ti atom and four N_3 moieties (Fig. 3, I_7 and I_8). We also considered structures composed of one Ti atom, one N_5 ring and one N_7 ring (N_5TiN_7) (Fig. 3, I_9), and one Ti and two N_6 rings (N_6TiN_6) (Fig. 3, I_{10}). After full relaxation, it was found that, for the neutral cluster, the initial structures of I_1, I_2 and I_3 converged to the same structure with D_{3d} symmetry, labeled as N_{1-3} in Fig. 3, which is the lowest energy geometrical configuration with a magnetic moment of 2.0 μ_B. While the other optimized isomers, labeled as $N_4 \sim N_{10}$ in Fig. 3, have much higher energies than isomer N_{1-3}. Their relative energies, calculated with respect to the lowest energy configuration, and symmetries are also given in Fig. 3. In the lowest energy geometry (N_{1-3}), the Ti–N_2 distance and N–N bond length are 2.09 and 1.12 Å, respectively. The average binding energy of each N_2 molecule with Ti in isomer N_{1-3} is 0.79 eV, which is larger than that in TiN_2. The $Ti(N_3)_4$ structure with T_d symmetry is 6.18 eV higher in energy than the most stable $Ti(N_2)_6$ complex. The linear Ti–N–NN bond angles of the T_d structure calculated in this work are in agreement with those obtained from previous theoretical calculations on free gaseous $Ti(N_3)_4$.[37,38] These bond angles were found to vary in the solid phase due to solid-state effects.[25] The N_5TiN_7 structure has a Ti atom sandwiched by an η^5-N_5 ring and an η^7-N_7 ring, similar to that reported by Gagliardi and Pyykkö.[10] It is worth mentioning that η^5–η^7 sandwich structures were also observed in $(C_5H_5)M(C_7H_7)$ type compounds, where M is a transition metal.[52–54] The N_6TiN_6 structure exhibits D_{2d} symmetry, in which the two N_6 rings are distorted and only two N atoms in each N_6 ring interact directly with the Ti atom, with a shorter Ti–N distance of 1.98 Å. The N_5TiN_7 and N_6TiN_6 structures are higher in energy than the most stable $Ti(N_2)_6$ complex by 13.65 and 14.89 eV respectively. According to the calculated binding energies, the decomposition of $Ti(N_3)_4$, N_5TiN_7, and N_6TiN_6 into a Ti atom and six N_2 molecules could release energies of 139, 857, and 978 kJ mol^{-1} respectively.

For the cationic TiN_{12}^+ cluster, the initial structures of I_1, I_2, I_3 and I_4 converged to one structure (P_{1-4}) with O_h symmetry, as shown in Fig. 3. This is the lowest energy configuration of TiN_{12}^+ with a Ti^+–N_2 distance and N–N bond length of 2.17 and 1.11 Å, respectively. The magnetic moment was found to be 3.0 μ_B. The

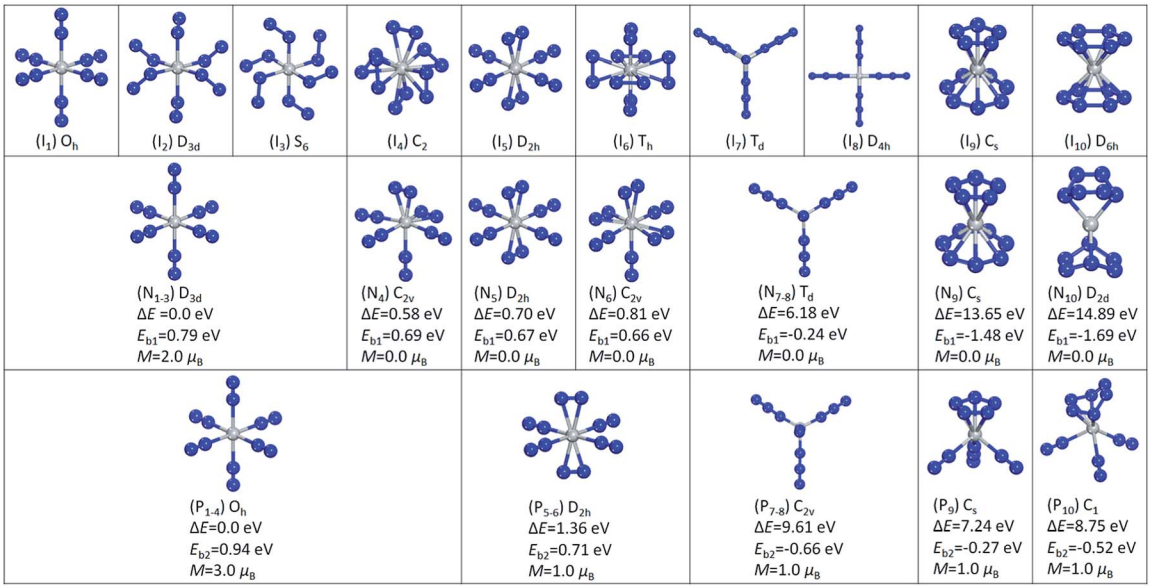

Fig. 3 Ten initial structural isomers of TiN_{12} (I_1–I_{10}). Optimized structures and the corresponding relative energies ΔE calculated with respect to the lowest energy structures N_{1-3} and P_{1-4}, average binding energies E_{b1} and E_{b2}, and magnetic moments of the neutral TiN_{12} (N_1–N_{10}) and TiN_{12}^+ (P_1–P_{10}).

average binding energy of each N_2 with Ti in isomer P_{1-4} was calculated to be 0.94 eV. The other optimized isomers, namely P_{5-6}, P_{7-8}, P_9 and P_{10} in Fig. 3, were found to be higher in energy than isomer P_{1-4} by 1.36, 9.61, 7.24 and 8.75 eV, respectively. The structure of $Ti(N_3)_4^+$ has C_{2v} symmetry. The N_5TiN_7 and N_6TiN_6 structures of TiN_{12}^+ are not stable. The N_5TiN_7 structure is rearranged into a $N_5Ti(N_3)(N_2)_2$ type of structure, while the N_6TiN_6 structure is rearranged into $N_6Ti(N_2)_3$ after the geometry optimizations. According to the calculated binding energies, the decomposition of $Ti(N_3)_4^+$, $N_5Ti(N_3)(N_2)_2^+$, and $N_6Ti(N_2)_3^+$ can release energies of 382, 156, and 301 kJ mol^{-1}, respectively.

5 Discussion

5.1 Comparison of binding energies

Based on the calculated binding energy of the most stable structure of the TiN_{12}^+ cluster (0.94 eV), the energy of a 532 nm photon is able to dissociate two N_2 molecules from isomer P_{1-4}, while the energy of a 266 nm photon is able to dissociate four N_2 molecules. This is in good agreement with our photodissociation experiment, as the experiment showed that the photodissociation of TiN_{12}^+ at 532 nm could remove at least 4 nitrogen atoms (two N_2 molecules), and photodissociation at 266 nm could remove at least 8 nitrogen atoms (four N_2 molecules). The detection of no photofragments at 1064 nm indicates that the energy barrier for the dissociation of TiN_{12}^+ is higher than 1.16 eV. In the experiment, the production of TiN_6^+, TiN_4^+, TiN_2^+ and Ti^+ fragments at 532 nm, and the production of TiN_2^+ and Ti^+ fragments at 266 nm are probably due to multiple-photon processes. The good agreement between the experiment and the theoretical calculations validates the theoretical method selected for this work and confirms that the TiN_{12}^+ cluster detected in our experiment has the form $Ti(N_2)_6^+$ with O_h symmetry. This is consistent with the matrix infrared and ultraviolet-visible spectroscopy studies of $Ti(CO)_6$ and $Ti(N_2)_6$ by Busby *et al.*[55]

Although the binding energy of neutral TiN_2 (0.25 eV) is smaller than that of TiN_2^+ (0.93 eV) by 0.68 eV, the Ti–N bond in neutral TiN_2 (1.94 Å) is actually shorter (stronger) than that in TiN_2^+ (2.18 Å), while the N–N bond in neutral TiN_2 (1.15 Å) is longer (weaker) than that in TiN_2^+ (1.11 Å). The decrease in the binding energy for neutral TiN_2 compared to TiN_2^+ is due to the weakening of the N–N bond. Thus, we would like to stress that the calculated binding energies do not reflect the exact Ti–N bond strengths in the clusters. The N–N bond in TiN_2^+ is weaker than that in the N_2 molecule; thus, the Ti–N bond strength in TiN_2^+ would be larger than the binding energy (0.93 eV). Moreover, the Ti–N bond in neutral TiN_2 is stronger than the Ti–N bond in TiN_2^+. Hence, we obtain the relation: BE[(Ti–N)TiN_2] > BE[(Ti–N)TiN_2^+] > 0.93 eV, where BE[(Ti–N)TiN_2] is the Ti–N bond energy in TiN_2 and BE[(Ti–N)TiN_2^+] is the Ti–N bond energy in TiN_2^+. This also implies that the N–N bond in neutral TiN_2 is weaker than those in TiN_2^+ and N_2 by at least 0.68 eV, which can be formularized as: BE[(N–N)TiN_2] + 0.68 eV < BE[(N–N)TiN_2^+] < BE[(N–N)N_2], where BE[(N–N)TiN_2], BE[(N–N)TiN_2^+], and BE[(N–N)N_2] are the N–N bond energies in TiN_2, TiN_2^+ and N_2, respectively.

Similarly, although the average binding energy of the most stable structure of TiN_{12} (0.79 eV) is smaller than that of TiN_{12}^+ (0.94 eV) by 0.15 eV, the Ti–N bonds in neutral TiN_{12} (2.09 Å) are actually shorter (stronger) than those in TiN_{12}^+ (2.17 Å), while the N–N bonds in neutral TiN_{12} are longer (weaker) (1.12 Å) than those in TiN_{12}^+ (1.11 Å). We can also conclude that the Ti–N bond energies of both TiN_{12} and TiN_{12}^+ are larger than 0.94 eV, BE[(Ti–N)TiN_{12}] > BE[(Ti–N)TiN_{12}^+] > 0.94 eV.

It is interesting to note that the average binding energy of each N_2 with Ti in the ground state of neutral TiN_{12} is 0.79 eV, which is much larger than that in TiN_2, while the average binding energy of each N_2 with Ti^+ in the ground state of TiN_{12}^+ is 0.94 eV, which is nearly the same as that in TiN_2^+. Considering the bond lengths in TiN_2, TiN_{12}, TiN_2^+, and TiN_{12}^+, we can see that the Ti–N bond lengths are in the order $TiN_2^+ \approx TiN_{12}^+ > TiN_{12} > TiN_2$, while the N–N bond lengths are in the order $TiN_2^+ \approx TiN_{12}^+ < TiN_{12} < TiN_2$. The Ti–N and N–N distances in TiN_2^+ and TiN_{12}^+ are very close to each other, while those in TiN_2 and TiN_{12} are very different from each other. The Ti–N bond in TiN_2 is much shorter than those in the other three species, and the N–N bond in TiN_2 is much longer than those in the other species. In TiN_2, the N–N bond is weakened significantly due to the strong Ti–N_2 interaction. This could explain why the calculated binding energies of TiN_2^+ and TiN_{12}^+ are similar while the binding energy of TiN_2 is much smaller than that of TiN_{12}. Overall, we have BE[(Ti–N)TiN_2] > BE[(Ti–N)TiN_{12}] > BE[(Ti–N)TiN_{12}^+] > BE[(Ti–N)TiN_2^+] > 0.93 eV.

5.2 NBO analyses

To further address the differences in the binding energies, we performed NBO analyses for TiN_2, TiN_2^+, TiN_{12} and TiN_{12}^+ in order to understand the effects of charge and coordination number on the binding and electronic structures. The calculated results are provided in Tables S1–S4.† Based on the NBO data, we note that in neutral TiN_2, the Ti lone pairs in the spin-up channel with d-orbital components of 99.51% donate 0.64 electrons to the π-antibonding orbitals between the two N atoms, which have p-orbital components of 99.90% and 99.53%. The corresponding back donations from the N valence lone pairs in two spin channels to the valence non-Lewis lone pairs on Ti total 0.14 electrons, giving rise to the loss of approximately 0.50 electrons on the Ti site, while the N1 and N2 atoms gain 0.45 and 0.05 electrons, respectively. Thus, the Ti–N interaction is very strong and the N–N bond is weakened significantly in neutral TiN_2 because of the large charge transfer between Ti and N1. On the other hand, in TiN_2^+, the charge donation from the lone pair on Ti to the antibonding orbital of N_2 is negligible since it is more difficult to transfer electrons from Ti^+. Contrarily, about 0.09 electrons are transferred from the lone pair on N1 to Ti. N1 and N2 carry charges of −0.242 and +0.216 respectively, forming a dipole which strongly interacts with Ti^+, with a charge of +1.026, resulting in a large binding energy for N_2 and Ti^+.

On going from TiN_2 to $Ti(N_2)_6$, the enhanced coordination field splits the Ti 3d orbitals to form bonding orbitals between Ti and the six linking N1 atoms in both spin-up and spin-down channels. The bonding orbitals have Ti 4s, Ti 4p and Ti 3d components of 16.66%, 49.92% and 33.34% respectively, resulting in sp^3d^2 hybridization character, which is consistent with the octahedral ligand field where the Ti atom is located. Therefore, the bonding orbitals between Ti and N1 give rise to a larger binding energy for the N_2 molecule in $Ti(N_2)_6$ compared to that in TiN_2.

Despite their different charges, TiN_{12} and TiN_{12}^+ share some common features: (1) bonding orbitals are formed between Ti and N1, and between Ti^+ and N1; and (2) the second order perturbation analysis suggests that there are no obvious stabilization interactions associated with charge transfer between Ti and N_2. These two common features result in a reduction in the difference between the binding energies (0.79 *versus* 0.94 eV) of the N_2 molecules in the neutral and charged TiN_{12}.

5.3 Electronic and magnetic properties

In the lowest energy structure of cationic TiN_{12}, Ti^+ is six-fold coordinated with O_h symmetry, in which the five d orbitals of Ti split into three-fold degenerate d_{xy}, d_{xz} and d_{yz}, and two-fold degenerate $d_{x^2-y^2}$ and d_{z^2} orbitals. The former three orbitals are occupied by three spin-up electrons, while the latter two fold degenerate orbitals are empty, resulting in a magnetic moment of 3.0 μ_B. The energy gap between the highest occupied molecular orbitals (HOMOs) and lowest unoccupied molecular orbitals (LUMOs) is 2.8 eV, as shown in Fig. 4(b). However, compared to TiN_{12}^+, the neutral TiN_{12} cluster has one more electron, which would induce the Jahn–Teller effect. The symmetry changes from O_h to D_{3d}, and three electrons are spin-up and one electron is spin-down, leading to a total magnetic moment of 2.0 μ_B and an energy gap of 1.5 eV, as shown in Fig. 4(a). The three occupied spin-up orbitals, one occupied spin-down orbital, and two-fold degenerate lowest unoccupied molecular orbitals of neutral TiN_{12} are plotted in Fig. 5(a–f), and the Ti 3d-orbital component percentages are 38.3%, 38.3%, 50.6%, 58.3%, 65% and 65%, respectively. For comparison, the three-fold degenerate HOMOs and the three-fold degenerate LUMOs of TiN_{12}^+ are given in Fig. 5(g–l), and the Ti 3d-orbital component percentages are 41.6%, 41.6%, 41.6%, 78.0%, 78.0% and 78.0%, respectively. This suggests that the Ti 3d orbitals make a larger contribution to the frontier orbitals in the charged cluster (TiN_{12}^+) compared with the neutral TiN_{12}.

As discussed above, TiN_{12} and TiN_{12}^+ have magnetic moments of 2.0 and 3.0 μ_B, respectively. In order to see how the magnetic moments are distributed in the clusters, spin density

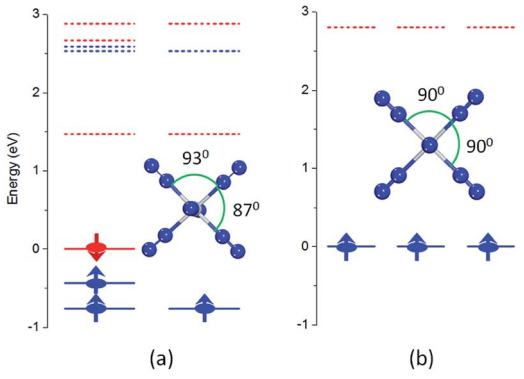

Fig. 4 Energy levels and optimized structures of TiN_{12} (a) and TiN_{12}^+ (b). The solid and dashed lines represent occupied and unoccupied energy levels, respectively. The blue and red colors represent spin-up and spin-down, respectively. The Fermi level is set to zero eV.

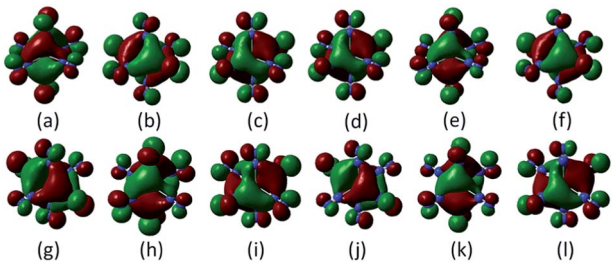

Fig. 5 Occupied orbitals and LUMOs of TiN_{12} (a–f) and TiN_{12}^+ (g–l).

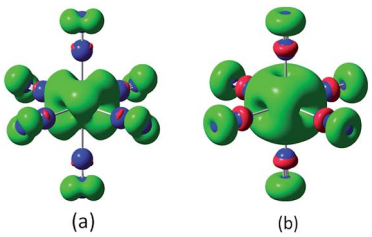

Fig. 6 Spin density distributions of TiN_{12} (a) and TiN_{12}^+ (b) (isosurface value is 0.004).

isosurfaces are plotted in Fig. 6. They clearly show that the spin density of TiN_{12}^+ is more symmetric, and that Ti^+ carries a larger net spin moment and more strongly polarizes the contacting N atoms (termed N1 atoms) antiferromagnetically. The non-contacting N atoms (named N2 atoms) are ferromagnetically polarized in both the neutral and charged clusters.

6 Conclusions

The TiN_{12}^+ cluster was generated experimentally and was further investigated by photodissociation experiments at 1064, 532, and 266 nm. The results showed that the TiN_{12}^+ cluster has very high abundance compared to other TiN_n^+ clusters. Density functional calculations were conducted to investigate the stable structures of TiN_{12}^+ and its corresponding neutral cluster TiN_{12}. The calculated binding energy of the TiN_{12}^+ cluster was in good agreement with the photodissociation experiment. The theoretical calculations found that the most stable structure of TiN_{12}^+ is $Ti(N_2)_6^+$ with O_h symmetry and the most stable structure of neutral TiN_{12} is $Ti(N_2)_6$ with D_{3d} symmetry. The Ti–N bond strengths are greater than 0.94 eV in both $Ti(N_2)_6^+$ and its neutral counterpart. The interaction between Ti and N_2 weakens the N–N bond significantly. The C_{2v} azide isomer $Ti(N_3)_4^+$ is higher in energy than the O_h $Ti(N_2)_6^+$ isomer by 9.61 eV. The azide isomer $Ti(N_3)_4$ and the N_5TiN_7 and N_6TiN_6 structures are higher in energy than the most stable $Ti(N_2)_6$ complex by 6.18, 13.65 and 14.89 eV respectively, indicating that the N_5TiN_7 and N_6TiN_6 isomers are potential candidates for high energy density materials.

Acknowledgements

This work was supported by grants from the Knowledge Innovation Program of the Chinese Academy of Sciences (Grant no. KJCX2-EW-H01), and the National Natural Science Foundation of China (NSFC-21273246, NSFC-51471004 and NSFC-11174014).

Notes and references

1 P. C. Samartzis and A. M. Wodtke, *Int. Rev. Phys. Chem.*, 2006, **25**, 527–552.
2 B. M. Rice, E. F. C. Byrd and W. D. Mattson, in *High Energy Density Materials*, ed. T. M. Klapotke, 2007, vol. 125, pp. 153–194.
3 Y. Li and S. Pang, *Chin. J. Explos. Propellants*, 2012, **35**, 1–8.
4 M. N. Glukhovtsev, H. J. Jiao and P. V. Schleyer, *Inorg. Chem.*, 1996, **35**, 7124–7133.
5 D. A. Dixon, D. Feller, K. O. Christe, W. W. Wilson, A. Vij, V. Vij, H. D. B. Jenkins, R. M. Olson and M. S. Gordon, *J. Am. Chem. Soc.*, 2004, **126**, 834–843.
6 K. O. Christe, *Propellants, Explos., Pyrotech.*, 2007, **32**, 194–204.
7 K. O. Christe, W. W. Wilson, J. A. Sheehy and J. A. Boatz, *Angew. Chem., Int. Ed.*, 1999, **38**, 2004–2009.
8 F. Cacace, G. de Petris and A. Troiani, *Science*, 2002, **295**, 480–481.
9 L. Gagliardi and P. Pyykkö, *J. Am. Chem. Soc.*, 2001, **123**, 9700–9701.
10 L. Gagliardi and P. Pyykkö, *J. Phys. Chem. A*, 2002, **106**, 4690–4694.
11 M. Straka and P. Pyykko, *Inorg. Chem.*, 2003, **42**, 8241–8249.
12 M. M. Doeff, S. F. Parker, P. H. Barrett and R. G. Pearson, *Inorg. Chem.*, 1984, **23**, 4108–4110.
13 G. V. Chertihin, L. Andrews and M. Neurock, *J. Phys. Chem.*, 1996, **100**, 14609–14617.
14 G. V. Chertihin, L. Andrews and C. W. Bauschlicher, *J. Am. Chem. Soc.*, 1998, **120**, 3205–3212.
15 A. Citra and L. Andrews, *J. Am. Chem. Soc.*, 1999, **121**, 11567–11568.
16 L. R. Brock and M. A. Duncan, *J. Chem. Phys.*, 1995, **102**, 9498–9505.
17 L. R. Brock and M. A. Duncan, *J. Phys. Chem.*, 1995, **99**, 16571–16575.
18 D. L. Robbins, L. R. Brock, J. S. Pilgrim and M. A. Duncan, *J. Chem. Phys.*, 1995, **102**, 1481–1492.
19 S. H. Pullins, J. E. Reddic, M. R. France and M. A. Duncan, *J. Chem. Phys.*, 1998, **108**, 2725–2732.
20 E. D. Pillai, T. D. Jaeger and M. A. Duncan, *J. Am. Chem. Soc.*, 2007, **129**, 2297–2307.
21 E. D. Pillai, T. D. Jaeger and M. A. Duncan, *J. Phys. Chem. A*, 2005, **109**, 3521–3526.
22 X. Yang, I. Gerasimov and P. J. Dagdigian, *Chem. Phys.*, 1998, **239**, 207–221.
23 I. A. Al-Jihad, B. Liu, C. J. Linnen and J. V. Gilbert, *J. Phys. Chem. A*, 1998, **102**, 6220–6226.
24 F. Y. Liu, X. Q. Zeng, H. P. Zhang, L. P. Meng, S. J. Zheng, M. F. Ge, D. X. Wang, D. K. W. Mok and F. T. Chau, *Chem. Phys. Lett.*, 2006, **419**, 213–216.
25 R. Haiges, J. A. Boatz, S. Schneider, T. Schroer, M. Yousufuddin and K. O. Christe, *Angew. Chem., Int. Ed.*, 2004, **43**, 3148–3152.

26 R. Haiges, J. A. Boatz, T. Schroer, M. Yousufuddin and K. O. Christe, *Angew. Chem., Int. Ed.*, 2006, **45**, 4830–4835.
27 R. Haiges, J. A. Boatz, M. Yousufuddin and K. O. Christe, *Angew. Chem., Int. Ed.*, 2007, **46**, 2869–2874.
28 R. Haiges, J. A. Boatz and K. O. Christe, *Angew. Chem., Int. Ed.*, 2010, **49**, 8008–8012.
29 R. Haiges, J. A. Boatz, R. Bau, S. Schneider, T. Schroer, M. Yousufuddin and K. O. Christe, *Angew. Chem., Int. Ed.*, 2005, **44**, 1860–1865.
30 A. C. Filippou, P. Portius, D. U. Neumann and K.-D. Wehrstedt, *Angew. Chem., Int. Ed.*, 2000, **39**, 4333–4336.
31 P. Portius, A. C. Filippou, G. Schnakenburg, M. Davis and K.-D. Wehrstedt, *Angew. Chem., Int. Ed.*, 2010, **49**, 8013–8016.
32 A. C. Filippou, P. Portius and G. Schnakenburg, *J. Am. Chem. Soc.*, 2002, **124**, 12396–12397.
33 T. M. Klapötke, B. Krumm, P. Mayer and I. Schwab, *Angew. Chem., Int. Ed.*, 2003, **42**, 5843–5846.
34 C. Knapp and J. Passmore, *Angew. Chem., Int. Ed.*, 2004, **43**, 4834–4836.
35 T. M. Klapötke, B. Krumm, M. Scherr, R. Haiges and K. O. Christe, *Angew. Chem., Int. Ed.*, 2007, **46**, 8686–8690.
36 A. Villinger and A. Schulz, *Angew. Chem., Int. Ed.*, 2010, **49**, 8017–8020.
37 L. Gagliardi and P. Pyykkö, *Inorg. Chem.*, 2003, **42**, 3074–3078.
38 Q. S. Li and H. X. Duan, *J. Phys. Chem. A*, 2005, **109**, 9089–9094.
39 L. Gagliardi and P. Pyykkö, *Theor. Chem. Acc.*, 2003, **110**, 205–210.
40 M. Straka, *Chem. Phys. Lett.*, 2002, **358**, 531–536.
41 H.-X. Duan and Q.-S. Li, *Chem. Phys. Lett.*, 2006, **432**, 331–335.
42 L. Jin and Y.-h. Ding, *J. Phys. Chem. A*, 2009, **113**, 5246–5250.
43 L. Jin and Y.-h. Ding, *J. Phys. Chem. A*, 2009, **113**, 13645–13650.
44 J. Zhang, Z. Zeng, H.-Q. Lin and Y.-L. Li, *Sci. Rep.*, 2014, **4**, 4358.
45 Y. C. Zhao, Z. G. Zhang, J. Y. Yuan, H. G. Xu and W. J. Zheng, *Chin. J. Chem. Phys.*, 2009, **22**, 655–662.
46 M. J. Frisch, G. W. Trucks, H. B. Schlegel, G. E. Scuseria, M. A. Robb, J. R. Cheeseman, G. Scalmani, V. Barone, B. Mennucci, G. A. Petersson, H. Nakatsuji, M. Caricato, X. Li, H. P. Hratchian, A. F. Izmaylov, J. Bloino, G. Zheng, J. L. Sonnenberg, M. Hada, M. Ehara, K. Toyota, R. Fukuda, J. Hasegawa, M. Ishida, T. Nakajima, Y. Honda, O. Kitao, H. Nakai, T. Vreven, J. A. Montgomery Jr, J. E. Peralta, F. Ogliaro, M. Bearpark, J. J. Heyd, E. Brothers, K. N. Kudin, V. N. Staroverov, R. Kobayashi, J. Normand, K. Raghavachari, A. Rendell, J. C. Burant, S. S. Iyengar, J. Tomasi, M. Cossi, J. M. M. N. Rega, M. Klene, J. E. Knox, J. B. Cross, V. Bakken, C. Adamo, J. Jaramillo, R. Gomperts, R. E. Stratmann, O. Yazyev, A. J. Austin, R. Cammi, C. Pomelli, J. W. Ochterski, R. L. Martin, K. Morokuma, V. G. Zakrzewski, G. A. Voth, P. Salvador, J. J. Dannenberg, S. Dapprich, A. D. Daniels, O. Farkas, J. B. Foresman, J. V. Ortiz, J. Cioslowski and D. J. Fox, *Gaussian 09, Revision A.02*, Gaussian, Inc., Wallingford, CT, 2009.
47 P. C. Hariharan and J. A. Pople, *Theor. Chim. Acta*, 1973, **28**, 213–222.
48 V. A. Rassolov, J. A. Pople, M. A. Ratner and T. L. Windus, *J. Chem. Phys.*, 1998, **109**, 1223–1229.
49 *CRC Handbook of Chemistry and Physics*, ed. W. M. Haynes, 95th edn, 2014–2015.
50 A. E. Reed, L. A. Curtiss and F. Weinhold, *Chem. Rev.*, 1988, **88**, 899–926.
51 G. M. Daly and M. S. El-Shall, *J. Chem. Phys.*, 1994, **100**, 1771–1772.
52 W. Noh and G. S. Girolami, *Inorg. Chem.*, 2008, **47**, 535–542.
53 S. Büschel, T. Bannenberg, C. G. Hrib, A. Glöckner, P. G. Jones and M. Tamm, *J. Organomet. Chem.*, 2009, **694**, 1244–1250.
54 J. Niinistö, T. Hatanpää, M. Kariniemi, M. Mäntymäki, L. Costelle, K. Mizohata, K. Kukli, M. Ritala and M. Leskelä, *Chem. Mater.*, 2012, **24**, 2002–2008.
55 R. Busby, W. Klotzbuecher and G. A. Ozin, *Inorg. Chem.*, 1977, **16**, 822–828.